EVALUATION OF THE COMPRESSIVE MECHANICAL PROPERTIES OF CELLULAR DMLS STRUCTURES FOR BIOMEDICAL APPLICATIONS

T. C. Dzogbewu*[1], L. Monaheng[2], J. Els, I. van Zyl, W. B. du Preez, I. Yadroitsava, I. Yadroitsev

Department of Mechanical and Mechatronic Engineering, Central University of Technology, Free State, Bloemfontein, South Africa
thydzo@yahoo.fr
jels@cut.ac.za
ivanzyl@cut.ac.za
lmonaheng@cut.ac.za
wdupreez@cut.ac.za
iyadroitsava@cut.ac.za
iyadroitsau@cut.ac.za

ABSTRACT

The type of material used in biomedical applications depends on specific implant applications; different types of implant need different mechanical properties. Since the architectures of bone tissues in the human body are not completely dense and solid, it is desirable to produce biomimic structures as a replacement for damaged bone tissues. Learning from nature, it can be understood that cellular structures would be more preferable for biomedical implants than dense solid structures. Verification of mechanical properties of DMLS PA 2200 cellular structures should be conducted since scaffolds from this material have been proven for biomedical applications. Ti6Al4V alloy is well known to have a superior track record as leading material for bone replacement since it is a light-weight and biocompatible material, but the density of human cortical bone is less than half that of solid Ti6Al4V implants. The mismatch of the elastic modulus between such implants and bone tissue is one of the major causes of stress shielding, bone resorption and implant loosening. Finite element analysis showed big differences in strains of jaw bone and an implanted solid Ti6Al4V part. The elastic modulus of lattice structures was used to simulate a complex mandible to obtain foreknowledge of manufacturing advanced light-weight implants with suitable biomechanical properties. Compressive properties of proposed cellular structures were determined to demonstrate the viability of attaining different effective elastic moduli for Ti6Al4V implants.

Keywords: direct metal laser sintering, mechanical properties, FEM, Ti6Al4V, Mandible implant

[1] The author is enrolled for D Eng degree in the Department of Mechanical and Mechatronic Engineering, Central University of Technology, Free state, South Africa
[2] The author is enrolled for M Tech degree in the Department of Mechanical and Mechatronic Engineering, Central University of Technology, Free state, South Africa.
* Corresponding author

1. INTRODUCTION

Additive manufacturing technologies such as Direct Metal Laser Sintering (DMLS) or Electron Beam Melting (EBM) are widely used for producing customized patient specific tailored devices. Using the undoubted capabilities of AM to produce cellular structures gives the designer total freedom in defining part geometry [1]. Most of the earlier research found in literature have focused on optimizing the DMLS process to manufacture dense non-porous parts [2], but more recently great attention has been given to manufacturing low-density lattice structures for biomedical applications [3-4].

In an era of high-speed automobiles, it is critical to produce energy absorbing implants for head injury patients. The natural parietal cranial bone is designed to absorb shock during an impact or crush. The irregularly porous structure of rod and plates like trabeculae at the middle of the two cortical bone surface layers serve as sink reservoir to prevent impact injury. In a case when the first outer cortical bone fractures the second still protects the brain before the cranial surgery. A biomimetic replacement is also required for cranial traumatic patients to minimized implant failure. The response of the head to traumatic loading is intrinsically linked to the anatomy and mechanical properties of the crania, hence any replacement which does not comprehensively take necessary anatomical consideration in the design process could lead to implant failure. As indicated by Singh et al. [5], three-dimensional open porous interconnected structures (scaffolds) can be used to repair or fill the defective bone sites of the human body. The earlier technologies did not permit manufacturing of graded biomimicry anatomical devices. But with the advent of AM technologies and the superior capabilities of the DMLS manufacturing process, it is most likely to manufacture implants with anatomical compatibility.

Using polyamide 12 (PA 2200) powder for AM of cranioplasty scaffolds has been proven by Zhang, et al., 2010; Wang, et al., 2007; Singh, et al., 2016 [5–7]. During in vitro cell culture tests it was shown that cell growth adherence and cell proliferation on the polyamide PA-2200 suggest the suitability of the scaffolds from this material. Now it is time to extend the goal posts by manufacturing exact anatomically tailored PA 2200 cranioplasty implants [5].

Ti6Al4V is one of the principal biomaterials for implants due to its high biocompatibility, good corrosion resistance and relatively low Young's Modulus as compared to other biometals [8]. Ti6Al4V alloy is the most extensively used for biomedical applications, however despite its celebrated biomechanical properties, it is well documented that the Young's modulus of AM Ti6Al4V alloy (110-114 GPa) is far above that of human bone (Table 1). Ohman *et al*. [9] found that a child's cortical bone tissue had significant lower compressive Young's modulus (−34%), yield stress (−38%) and ultimate stress (−33%) than an adult's bones.

Table 1. Mechanical properties of adult human bones [10]

	Cortical bone		*Cancellous bone*
	longitudinal direction	*transverse direction*	
Tensile strength, MPa	79-151	51-56	
Compressive strength, MPa	131-224	106-133	2-5
Elastic moduli of compact bone, GPa	17-20	6-13	0.76-4
Apparent density, g/cm^3	1.99	0.05-1.0	

The mismatch of mechanical properties of the bone and implant can cause the displacement of the implant [11, 12]. In view of this, there is a need to produce novel biomaterial with better mechanical properties more similar to that of bone tissue and to use cellular structures for advanced implants. Since cellular structures are known to mimic the anisotropic porous nature of bone and with the possibility of tuning their elastic modulus over a wide range by varying the lattice properties [13], such structures would probably provide the much-needed solution by reducing the effective Young's modulus of Ti6Al4V alloy [14]. The creation of open space within the lattices would also translate to minimal material usage and the discrete

pore volumes in micron dimensions would in addition produce a perfect surface for bone-implant interlocking with suitable biomechanical properties [15].

Table 2 presents values of porosity and elastic modulus of various forms of AM Ti6Al4V cellular structures. Wieding et al. [16] used DMLS to manufacture Ti6Al4V cellular structures of different geometry with an approximate porosity of 70%. The Young's modulus for the compression test was in the range of 3.7–6.7 GPa and the ultimate compressive strength (UCS) 145–164 MPa. It was shown that a low elastic modulus can stimulate growth of bone cells due to mechanical stimulus by physiological load application, and avoid stress shielding caused by high stiffness gradients between bones and implants.

Table 2: Mechanical properties of DMLS and EBM Ti6Al4V cellular structures

Type of lattice structure	*Technology*	*Porosity, %*	*Young's Modulus (GPa)*	*Reference*
Scaffold with rectangular struts	DMLS	70.2 ± 0.4	5.1±0.3	[16]
Scaffolds with shifted strut alignment		71.9 ± 0.2	3.7±0.2	
Scaffolds with diagonal struts		68.7 ± 0.2	6.7±0.3	
Unit cell in the form of prisms	DMLS	69	0.341	[3]
Diamond structure	EBM	80.5	1.6	[17]
Hatched structure		59.5	12.9	
Honeycomb-like structure	EBM	66.3	2.5	[18]
Rhombic dodecahedron	EBM	70.32	2.13	[19]
Rhombic dodecahedron		60.41	2.68	
Rhombic dodecahedron		50.75	2.92	

Very recently, de Damborenea [3] also manufactured cellular Ti6Al4V structures and obtained a Young's modulus of 0.341 GPa. Parthasarathy et al. [19] also focused on investigating the compressive strength and Young's modulus of Ti6Al4V lattice structures for biomedical applications by the EBM process and obtained Young's modulus values between 0.57-2.92 GPa and compressive strength of 7.28-163 MPa for lattice structures of varying porosity. Murr, et al. [15] experimented on Ti6Al4V lattice structures by EBM technology and obtained Young's modulus values of 0.9-1.5 GPa for samples with 82% porosity. Heinl et al. [17] also obtained Young's modulus values of 1.6-12.9 GPa for different geometrical lattice structures of Ti6Al4V alloy. The experimental investigation of Li et al. [18] produced a Young's modulus of 2.5±0.5 GPa for Ti6Al4V lattice structures. The choice of structure type has to be based on lattice structures that produce elastic modulus close to that of cortical or trabecular bone (Table 1).

In this study finite element modelling was used to demonstrate how modification of the elastic modulus of different parts of a Ti6Al4V mandibular implant could lead to closer matching with the mechanical properties of human bone, while still retaining the required strength for normal functionality. Subsequently, the mechanical properties of selected cell structures were determined to demonstrate the extent to which the effective elastic modulus of Ti6Al4V could be modified to approach that of bone through selection of appropriate cellular lattice structures.

2. MODELLING OF MANDIBLE IMPLANTS

The human mandible (lower jaw) is noted as the strongest bone of the skull and is capable of moving independently from the head movement. It supports the lower teeth and provides a place of attachment for the mastication muscles [20]. The masseter muscle is the principal mastication muscle and is responsible for retracting and elevating the mouth (opening and closing of the mouth). It must be able to exert enough force for biting and chewing of food [21]. The magnitude of the resultant force produced by the mastication muscles on the dental

arches during clenching of the teeth in maximum intercuspation for normal humans ranges from 246.9 to 2091.9 N [22]. The resultant force during clenching of the teeth was found to act at an angle of approximately 69° to the occlusal plane (see Fig. 1(b). This is because the angle between the occlusal plane and the anterior boarder of the masseter muscle remains approximately 69^0 (Fig.1(b) point D) based on the cephalogram analysis of Sato, et al. [23].

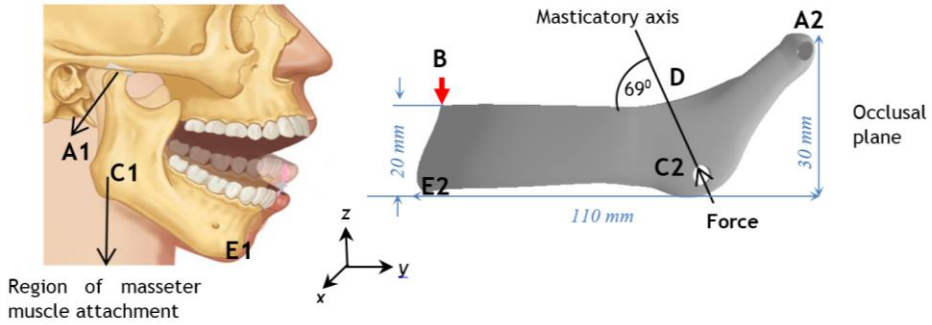

(a) (b)

Fig.1. Symmetry representation of the mandible (a) and a CAD model (b).

The developed model was resemble the geometry and function of the natural mandible (Fig.1a-b). The region A1 corresponds to region A2 in Fig.1. During finite element analysis (FEA) the implant was allowed to rotate about the point A2 as in normal clenching of the teeth (A1), but it could not translate or move up and down. The applied load during the simulation was applied at an angle of 69° (Fig.1b point C2) to mimic the function of the masseter muscle. Furthermore, the implant was fixed on a single node at point B (Fig. 1(b)) so that it could not translate nor rotate when performing the simulation. Since only half of the mandible was designed for this analysis, only half (1000 N) of the total resultant force exerted by the mastication muscle was used in the simulation. The hole at point C2 where the force is applied represents the location of the masseter muscle attachment (point C1 in Fig. 1(a)). Mandible numerical model had constant thickness of 2 mm.

To simulate the effect of the implants with different elastic moduli, FEA was performed on the models shown in Fig. 2. Model 1 of the mandible was assigned an elastic modulus of 11.7 GPa and Poisson's ratio of 0.35, both representing the properties of cortical bone. At the angle of incidence of the force, the model would experience the highest stress at the upper part 1 of the mandible indicated in Fig. 2(a). This correlates with the normal functioning of the mandible, since that is the part that translates around a fixed point (point A2 in Fig.1(b)) when it bears the maximum load during opening and closing of the mouth [20]. Consequently, upper part 1 is displays the largest strain. The force applied at point C2 is transmitted to section 2.

Section 2 of Model 2 (Fig. 2(b)) was designed to represent the properties of solid Ti6AlV implant (elastic modulus of 110 GPa and Poisson's ratio of 0.35), while the outer sections (sections 1 and 3) were assigned the elastic modulus and Poisson's ratio of cortical bone (11.7 GPa and 0.35, respectively). The Model 3 was similar to Model 2, but with elastic modulus of 30 GPa for the mid-section (Fig. 2(c)). This complex arrangement was meant to investigate the differences in strain (deformation) at the mid-portion (section 2) of the implant models and to ascertain its suitability for patients who may not need total mandible replacement but replacement only of a damaged part of their jaw bone. The model with the lower elastic modulus (Fig.2(c)) demonstrates a more uniform retrogressive deformation from region 1 to 2 than the one with the higher elastic modulus at the middle (Fig. 2(b)).

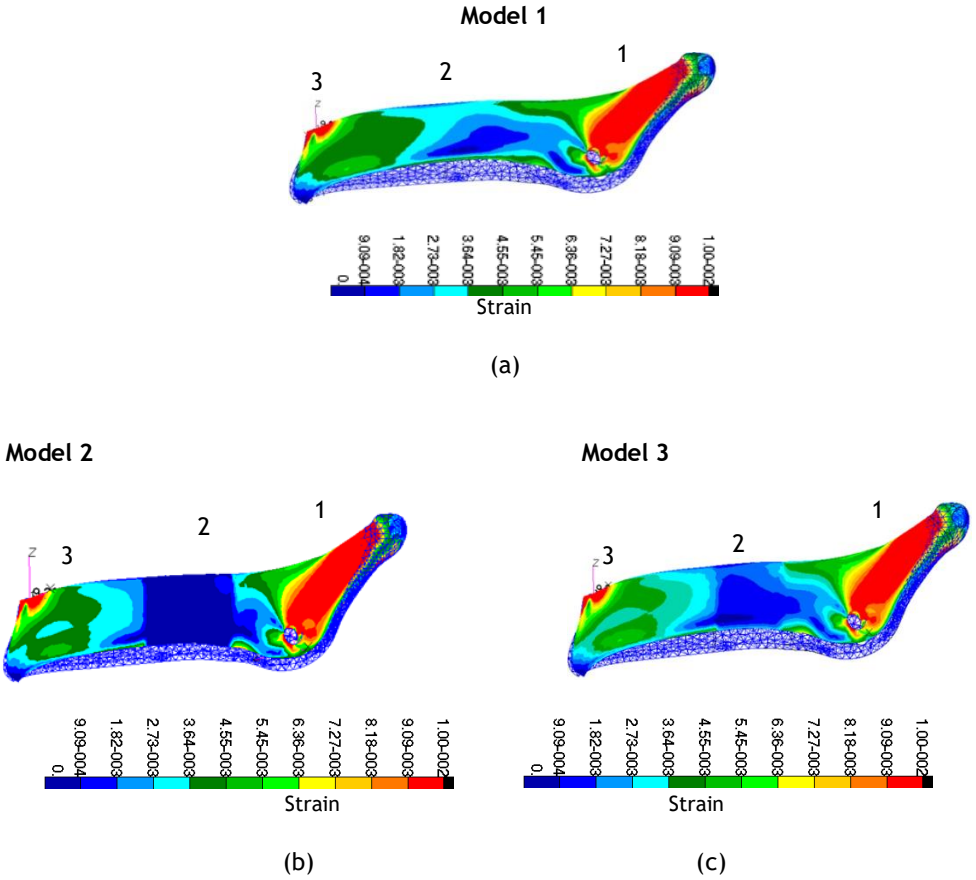

Fig.2: Numerical simulations for mandible models. True strains for bone: (a), with Ti6Al4V solid (b) and lattice structures (c).

For bone implant contact interlocking and avoidance of the stress shielding effect, replacing a damaged part of a mandible with a relatively lower elastic modulus is expected to prevent bone failure since the stresses and strains induced by the mastication forces would be transferred more uniformly from bone to implant. It is therefore possible to produce a complex mandible implant with a strong region (higher elastic modulus, section 1) that can bear the force exerted by the masseter muscle without fracture and a region with lower elastic modulus (sections 2-3, Figs. 1–2).

3. MATERIALS AND METHODS

The specimens for compression tests were cubes with periodic cellular lattice structures and solid top and bottom layers of 1 mm in thickness. Cubes with size 25x25x25 mm^3 were designed with 25%, 50% and 75% volume fraction with rhombic nodes (types A, B, C) and 2 cubes with similar size but 50% and 75% volume fraction (types D and E) (Fig. 3). Volume fraction was defined as the volume percentage of solid material in the CAD cellular lattice structure. A fixed unit cell size of 5 mm was chosen. The strut diameters of the unit cells are indicated in Fig. 3. Three cubes in each series were produced from PA 2200 powder (polyamide 12) by an EOS P380 machine.

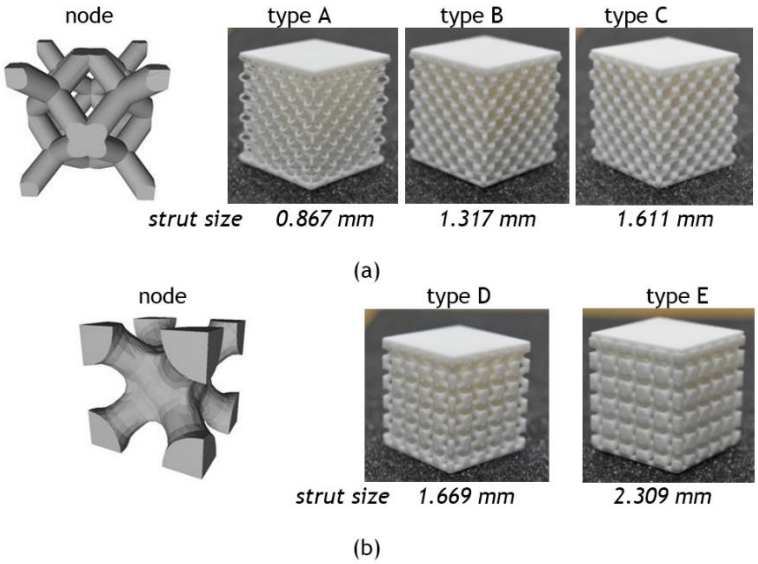

Fig.3. CAD models of nodes for cellular structures and PA 2200 cubes with rhombic (a) and diagonal cellular structures (b).

The chemical composition of the spherical argon-atomized Ti6Al4V (ELI) (-45 μm) powder from TLS Technik was the following (in wt.%): Ti (bal.), Al (6.34), V (3.94), O (0.058), N(<0.006), H(0.001), Fe (0.25), C(0.006), Y (<0.001). The 10th, 50th and 90th percentiles of equivalent diameter (weighted by volume) of the powder particles were d10=13 μm, d50=23 μm and d90=37 μm. The samples were produced by the EOSINT M280 system. The substrate and powder materials were similar in chemical composition. Argon was used as the protective atmosphere; the oxygen level in the chamber was 0.07-0.12%. Specimens attached to the substrate were subjected to heat treatment post-processing in Ar atmosphere at 650°C (3 hours) for stress relieving, then were separated from the base plate and cut into 4 parts each via wire Electrical Discharge Machining (Fig. 4).

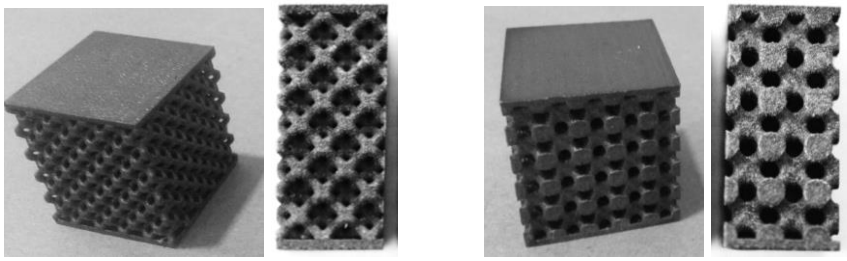

(a) (b)

Fig.4. General and frontal views of Ti6Al4V (ELI) DMLS objects with rhombic (a) and diagonal structures with 50% CAD volume fraction (b).

Mechanical properties of the Ti6Al4V and PA 2200 DMLS specimens were obtained through uniaxial compression tests. Compressive stress was calculated as ratio of load (N) to the top surface area in direct contact during compression tests. Compression tests for PA 2200 samples were carried out by an Instron 1342 servo-hydraulic testing machine under constant strain rate of 3.0 mm/min. Ti6Al4V samples were tested by an MTS Criterion Model 43 Electric testing system (30kN max load cell) under 0.3 mm/min strain rate.

4. RESULTS AND DISCUSSION

4.1 PA 2200 cellular structures

Stress-strain diagrams of compression tests for DMLS PA 2200 samples are shown in Fig. 5. Elastic moduli for manufactured cellular structures were calculated as chord 0.1–0.5 MPa for type A samples, 1–4 MPa for type B samples, 2–10 MPa for types C–E. The mechanical properties of the cellular structures measured from the compression test data are summarized in Table 3. The strain-stress behavior at compression was similar for both types of nodes, but diagonal scaffolds (samples D–E) were stiffer than rhombic structures (samples B–C).

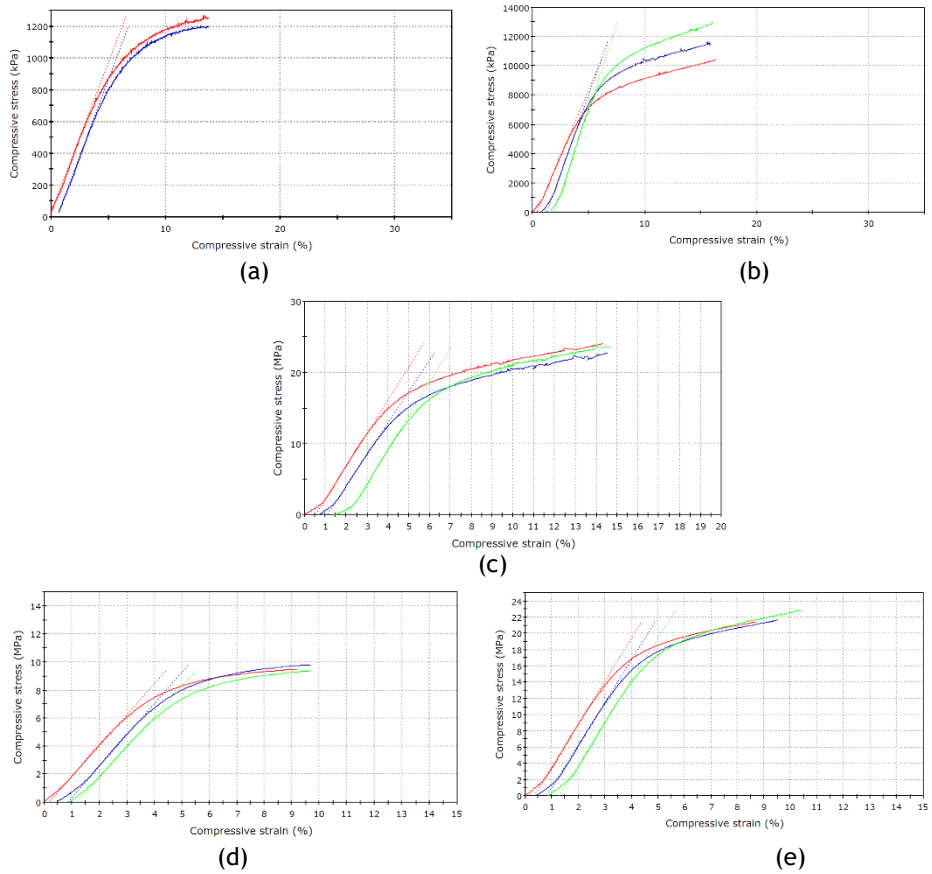

Fig. 5. Compressive characteristic diagrams for different DMLS PA 2200 cellular samples: a (type A), b (type B), c (type C), d (type D) and e (type E) series.

For solid DMLS PA 2200 samples obtained by Miron-Borzan et al. [24] elastic modulus was E_0=1.2–1.38 GPa. For 50% porous cellular structures, elastic modulus was about 6 times lower in comparison with solid material (Table 2). Gibson and Ashby [25] predicted the response to load for cellular structures as

$$\frac{E}{E_0} = k\left(\frac{\rho}{\rho_0}\right)^r$$

where E_0 and ρ_0 are elastic modulus and density for solid material, k and r depends on the type of structure. Fig. 6 shows the elastic modulus of DMLS PA 2200 cellular structures as a function of volume fraction and maximum strut size for rhombic and diagonal scaffolds at fixed unit cell size of 5 mm. The Young's modulus increases with the volume fraction, as was predicted by the Gibson–Ashby model. Compressive strength also increases with strut size, but more drastic changes were observed for the rhombic type nodes (Table 3, Fig. 6).

Table 3. Mechanical properties of different DMLS PA 2200 cellular samples

Types	*Relative CAD porosity, %*	*Maximum load, N*	*Elastic Modulus, MPa*	*Compressive stress at maximum compressive load, MPa*	*Compressive strain at maximum compressive load, %*
A	75	765±27	19±0.2	1.23±0.04	12.8±0.7
B	50	7384±816	208.5±24.4	11.69±1.3	15.2±1.0
C	25	15114±464	461.6±16.9	23.5±0.7	13.5±0.9
D	50	5917±150	219.2±4.3	9.5±0.2	9.0±0.2
E	25	14227±529	524.3±4.2	22.0±0.1	9.1±0.4

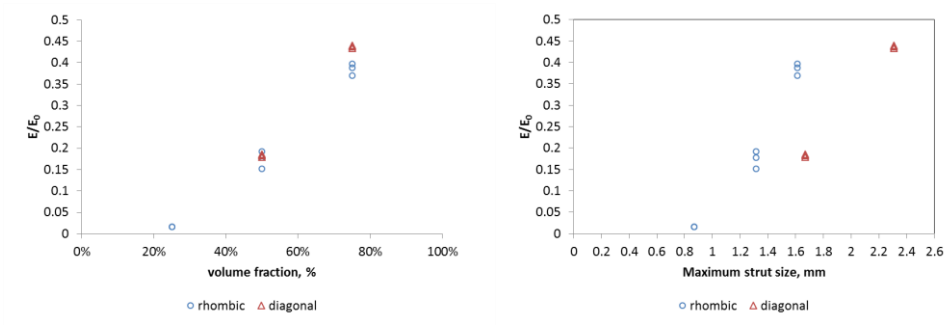

(a) (b)

Fig. 6. Elastic modulus *versus* volume fraction (a) and maximum strut size (b) of DMLS PA2200 cellular structures.

DMLS PA 2200 of 50-75% volume fraction cellular diagonal and rhombic structures had peak stress of 9.5-23.5 MPa. The proposed DMLS structures had stable mechanical properties and can be used in biomedical applications, depending on the required strength characteristics. Additional studies on regenerative properties of the tissue cells at the indicated shapes and sizes should be carried out.

4.2 Ti6Al4V (ELI) cellular structures

Stress-strain diagrams of compression tests for DMLS Ti6Al4V samples are shown in Fig. 7 and the resultant mechanical properties are presented in Table 4.

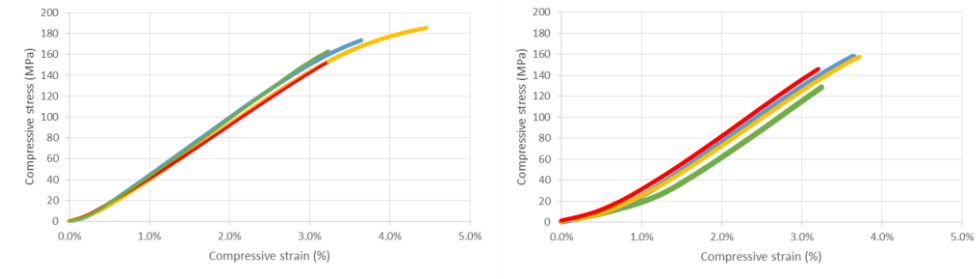

(a) (b)

Fig. 7. Compressive characteristic diagrams for Ti6Al4V cellular samples: structures of B (a) and D (b) types.

The macroscopic Young's modulus for Ti6Al4V cellular structures was estimated as the slope of the linear part of the compressive characteristic diagram. The yield stress, defined as the inflection point between the linear and non-linear parts of the stress-strain diagram, was about 140-160 MPa and higher (Fig. 7). Taking into account the trends from Fig. 6(a) and assuming similar behavior of DMLS cellular samples, manufacturing of 50% volume fraction will result in closely similar modulus of elasticity for the rhombic and diagonal structures for

the same unit cells. elastic moduli were found to be similar for the Ti6Al4V rhombic and diagonal scaffolds: 5.3 GPa and 5.1 GPa, respectively, as shown in Table 4.

Table 4. Mechanical properties of different DMLS Ti6Al4V cellular samples

Types	*Max load, kN*	*Elastic Modulus, GPa*	*Compressive stress at maximum load, MPa*	*Compressive strain at maximum load, %*
B	25	5.3±0.2	168.4±14.4	3.40±0.58
D	25	5.1±0.1	162.7±4.8	3.19±0.07

Phase transformations, texture effects and microstructural strengthening, as well as surface roughness, can affect the mechanical properties of the AM cellular structures [26]. The microstructure of as-built Ti6Al4V alloy typically consists of α´ martensite. After stress-relieving heat treatment no significant changes in the microstructures have been found. The microstructures of the nodes of the DMLS cellular structures are shown in Figures 8–9. Primary β grains were oriented almost parallel to the building direction (Fig. 8b, 9b); at perpendicular cross-sections the grain boundaries of the primary β phase also were well distinguished (Fig. 8a, 9a).

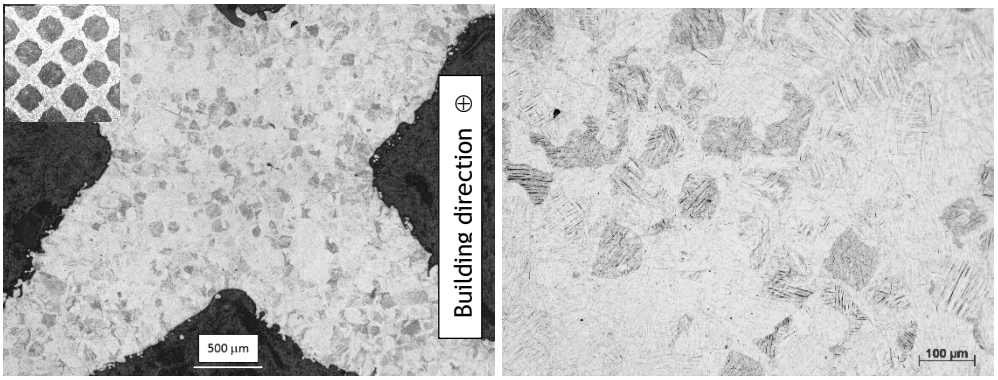

(a)

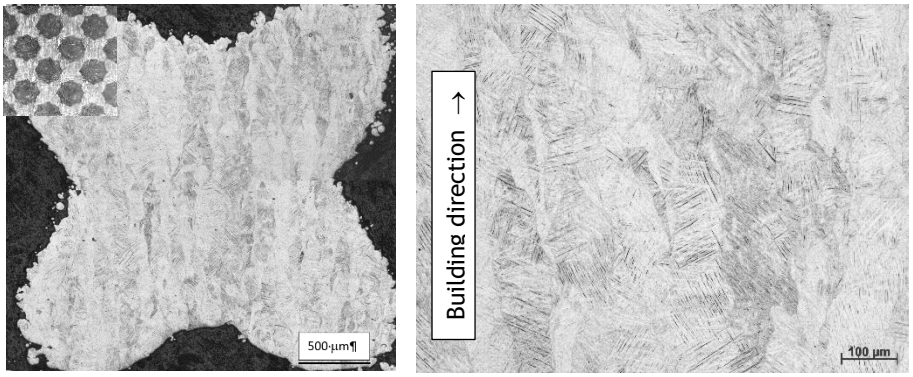

(b)

Fig. 8. Cross-sections of Ti6Al4V rhombic node (type B): perpendicular (a) and along building direction (b).

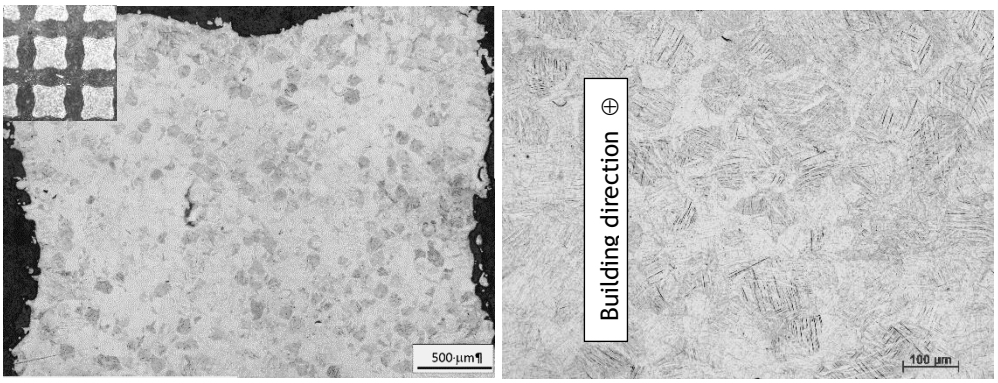

(a)

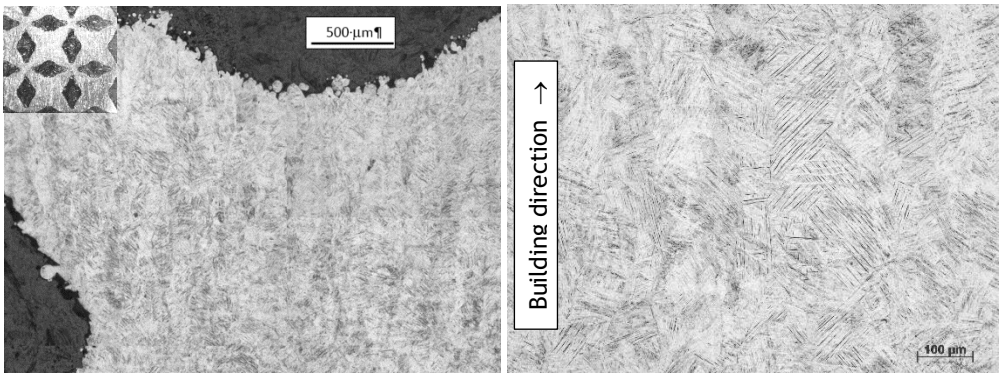

(b)

Fig. 9. Cross-sections of Ti6Al4V diagonal node (type D): perpendicular (a) and along building direction (b).

Attached powder particles inside the cellular structures are visible in the cross-sections (Figs. 8a–9a). No pores bigger than 20 µm were found in the analysed cross-sections of the struts.

DMLS material had stable mechanical properties when loading was applied co-axial to the building direction. Compressive tests showed that the proposed DMLS Ti6Al4V cellular structures are suitable for fabrication of light-weight implants because their mechanical properties are close to the properties of human bone (Tables 1 and 4).

5. CONCLUSION

When selecting the implant material to replace a part of a damaged bone, distinct differences between the Young's moduli of these materials could lead to bone/implant discontinuities resulting in interfacial failure. The finite element analysis clearly demonstrated that it would be worth designing and manufacturing complex implants based on the mechanical properties of cellular structures. Manufacturing complex implants with the inherent mechanical properties of lattice structures would definitely lead to advanced light-weight implants with biocompatible mechanical properties.

The elastic modulus as well as compressive strength of PA 2200 DMLS structures increased with strut size and volume fraction. Proposed geometry of cellular structures from this material can be used as scaffolds in regenerative surgery to repair the body quickly and effectively.

Ti6Al4V DMLS rhombic and diagonal cellular structures have elastic modulus and strength similar to the cancellous human bone. It must be noted that compression tests were made of uniaxially and cellular structures were tested along building direction. Further investigations of mechanical properties of DMLS cellular structures are needed to improve the elastic modulus and to achieve satisfactory strength with respect to the loading direction and required strength for the specific implants.

6. ACKNOWLEDGMENTS

This work is based on the research supported by the South African Research Chairs Initiative of the Department of Science and Technology and National Research Foundation of South Africa (Grant №97994) and the Collaborative Program in Additive Manufacturing (Contract №CSIR-NLC-CPAM-15-MOA-CUT-01). Mechanical testing has been performed in the mechanical testing laboratory of the CSIR and the authors are grateful to Chris McDuling.

REFERENCES

1. **Contuzzi, N., Campanelli, S. L., Casavola, C. & Lamberti, L.** 2013. Manufacturing and Characterization of 18Ni Marage 300 Lattice Components by Selective Laser Melting, *Materials*, 6(8), pp 3451-3468.
2. **Yadroitsev, I., Krakhmalev, P., Yadroitsava, I.** 2015. Hierarchical design principles of selective laser melting for high quality metallic objects, *Additive Manufacturing*, 7, pp 45-56.
3. **de Damborenea,J.J., Larosa, M.A., Arenas, M.A., Hernández-López, J.M., Jardini, A.L., Ierardi,M.C.F., Zavaglia,C.A., Maciel, F. R. & Conde, A.** 2015. Functionalization of scaffolds produced by direct metal laser for biomedical applications. *Materials & Design*, 83, pp 6-13.
4. **Wally,Z.J., van Grunsven,W., Claeyssens,F., Goodall , R. & Reilly, G.C.** 2015. Porous titanium for dental implant applications, *Metals*, 5(4), pp 1902-1920.
5. **Singh, J. P., Pandey, P. M. Verma, A. K.,** 2016. Fabrication of three dimensional open porous regular structure of PA-2200 for enhanced strength of scaffold using selective laser sintering, *Rapid Prototyping Journal*, 22(4), pp 752-765.
6. **Zhang, J.C., Lu, H.Y., Lv, G.Y., Mo, A.C., Yan, Y.G. & Huang C.** 2010. The repair of critical-size defects with porous hydroxyapatite/polyamide nanocomposite: an experimental study in rabbit mandibles. *International Journal of Oral and Maxillofacial Surgery*, 39(5), pp. 469-477.
7. **Wang, H., Li, Y., Zuo Y., Li J., Ma S., Cheng L.** 2007. Biocompatibility and osteogenesis of biomimetic nano-hydroxyapatite/polyamide composite scaffolds for bone tissue engineering. *Biomaterials*, 28(22), pp. 3338-3348.
8. **Kulkarni, M., Mazare, A., Schmuki, P., Iglič, A.** 2014. Biomaterial surface modification of titanium and titanium alloys for medical applications. *Nanomedicine*, 111, p. 111.
9. **Ohman,C., Baleani, M., Pani,C., Taddei, F., Alberghini, M., Viceconti, M. & Manfrini, M.** 2011. Compressive behaviour of child and adult cortical bone. *Bone*, 49(4), pp 769-776.
10. **Nouri, A., Hodgson, P.D. & Wen**, C., 2010. Biomimetic Porous Titanium Scaffolds for Orthopedic and Dental Applications. Mukherjee A. (Ed.). *Biomimetics, Learning From Nature*. chapter 21, Intech, pp 415-50.
11. **Doh, R.M., Pang, N.S,, Kim, K.D., Park, W**., 2011. Implant displacement into the mandible: an unusual complication during implant surgery. *Implant Dentistry*, 20(5):345-348.
12. **Lee, S.-C., Jeong, C.-H., Im, H.-Y., Kim, S.-Y., Ryu, J.-Y., Yeom, H.-Y., & Kim, H.-M.**, 2013. Displacement of dental implants into the focal osteoporotic bone marrow defect: a report of three cases, *Journal of the Korean Association of Oral and Maxillofacial Surgeons*, 39(2), 94–99.

13. **Soman, P., Lee, J.W., Phadke, A., Varghese, S., Chen. S**. 2012. Spatial tuning of negative and positive Poisson's ratio in a multi-layer scaffold, *Acta Biomaterialia*, 8(7), pp 2587-2594.
14. **Lin, W.S., Starr,T.L., Harris,B.t., Zandinejad, A. & Morton, D.** 2013. Additive manufacturing technology (direct metal laser sintering) as a novel approach to fabricate functionally graded titanium implants: preliminary investigation of fabrication parameters. *The International Journal of Oral & Maxillofacial implants*, 28(6), pp 1490-1495.
15. **Murr, L.E., Gaytan, S.M., Medina,F., Lopez,H., Martinez,E., Machado, B.I., Hernandez, D.H., Martinez,L., Lopez,M.I., Wicker, R.B. & Bracke, J.** 2010. Next generation biomedical implants using additive manufacturing of complex, cellular and functional mesh arrays. *Philosophical Transactions of the Royal Society of London A: Mathematical, Physical and Engineering Sciences*, 368(1917), pp 1999-2032.
16. **Wieding, J., Jonitz, A. & Bader, R.** 2012. The effect of structural design on mechanical properties and cellular response of additive manufactured titanium scaffolds, *Materials*, 5(8), pp 1336-1347.
17. **Heinl, P., Müller,K., Körner, C., Singer, R.F & Müller, F.A.** 2008.Cellular Ti–6Al–4V structures with interconnected macro porosity for bone implants fabricated by selective electron beam melting. *Acta Biomaterialia*, 4(5), pp 1536-1544.
18. **Li, X., Wang, C., Zhang, W. & Li, Y.** 2009. Fabrication and characterization of porous parts for biomedical applications using electron beam melting process, *Materials Letters*, 63(3), pp 403-405.
19. **Parthasarathy, J., Starly, B., Raman, S. & Christensen, A.** 2010. Mechanical evaluation of porous titanium (Ti6Al4V) structures with electron beam melting (EBM), *Journal of the Mechanical Behavior of Biomedical Materials*, 3(3), pp 249-259.
20. **Saladin, K. S.** 1998. *Anatomy & physiology*. s.l.:WCB/McGraw-Hill.
21. **Santana-Mora, U. M.-Í. A.-P. U., del Palomar, A. P., Banzo, J. C. & Mora, M. J.** 2014. Muscular activity during isometric incisal biting. *Journal of Biomechanics*, 47(16), pp 3891-3897.
22. **Hattori,Y., Satoh,C., Kunieda, T., Endoh,R., Hisamatsu, H. & Watanabe, M.** 2009. Bite forces and their resultants during forceful intercuspal clenching in humans. *Journal of Biomechanics*, 42(10), pp. 1533-1538.
23. **2Sato, M., Motoyoshi, M., Hirabayashi, M., Hosoi, K., Mitsui, N & Shimizu, N.** 2007. Inclination of the occlusal plane is associated with the direction of the masticatory movement path. The European *Journal of Orthodontics*, 29(1), pp 21-25.
24. **Miron-Borzan ,C.S., Dudescu, M.C., Elghany, K.A., Ceclan, V., Berce, P**., 2015. Analysis of mechanical proprieties of selective laser sintered polyamide parts obtained on different equipment, *Materiale Plastice*, 52 (1), pp 39-42
25. **Gibson, L.J., Ashby M.F.,** 1997. *Cellular Solids Structure and Properties*, Cambridge University Press, Cambridge.
26. **Hernández-Nava, E., Smith, C.J., Derguti, F.; Tammas-Williams, S., Léonard, F., Withers, P.J., Todd, I., Goodall, R.,** 2015. The effect of density and feature size on mechanical properties of isostructural metallic foams produced by additive manufacturing, *Acta Materialia*, 85, 387–395.